Journal of Alloys and Compounds 524 (2012) 22–25

Contents lists available at SciVerse ScienceDirect

Journal of Alloys and Compounds

journal homepage: www.elsevier.com/locate/jallcom

Crystal structure determination of solar cell materials: Cu_2ZnSnS_4 thin films using X-ray anomalous dispersion

Hiroshi Nozaki [a,*], Tatsuo Fukano [a], Shingo Ohta [a], Yoshiki Seno [a], Hironori Katagiri [b], Kazuo Jimbo [b]

[a] Toyota Central R&D Labs. Inc., 41-1 Yokomichi, Nagakute, Aichi 480-1192, Japan
[b] Nagaoka National College of Technology, 888 Nishikatakai, Nagaoka, Niigata 940-8532, Japan

ARTICLE INFO

Article history:
Received 5 October 2011
Received in revised form 23 January 2012
Accepted 24 January 2012
Available online 2 February 2012

Keywords:
Solar cell
CZTS
X-ray diffraction
Anomalous dispersion

ABSTRACT

The crystal structure of Cu_2ZnSnS_4 (CZTS) thin films fabricated by vapor-phase sulfurization was determined using X-ray anomalous dispersion. High statistic synchrotron radiation X-ray diffraction data were collected from very small amounts of powder. By analyzing the wavelength dependencies of the diffraction peak intensities, the crystal structure was clearly identified as kesterite. Rietveld analysis revealed that the atomic composition deviated from stoichiometric composition, and the compositions were Cu/(Zn + Sn) = 0.97, and Zn/Sn = 1.42.

1. Introduction

To reduce the use of fossil fuels, other energy sources such as solar energy must be developed. Solar cells are an attractive energy source, because they do not generate harmful emissions. Among several solar cell materials, the Si-based solar cell is the most widely used worldwide. However, it is necessary to develop non-Si-based solar cells due to a lack of highly pure Si sources. Therefore, we are developing new type of solar cell material, Cu_2ZnSnS_4 (CZTS) thin films [1,2]. CZTS thin films first formed the heterostructure device by Ito [3]. CZTS thin films are an ideal material for low cost solar cells because neither rare metals nor harmful elements are required. Although the conversion efficiency of a CZTS solar cell is a few percent, which is lower than that of Si-based solar cells (~20%), there is room to improve the efficiency by better design of the materials. There are two types of crystal structures observed in CZTS thin films: kesterite and stannite [4]. Both crystal systems are tetragonal, and the only difference between them is the position of their Cu and Zn atoms (see Fig. 1) as reported by Schorr [5,6]. It was revealed that the electronic band calculation for several isomorphic crystal structures depends on the crystal structure [7]. Since the crystal structure strongly affects a material's ability to produce electric power, it is very important to understand the crystal structure. However, it is very difficult to distinguish between kesterite and stannite crystal structures by Rietveld analysis using X-ray diffraction data, because the two structures are very similar. Although the neutron diffraction technique can more effectively distinguish between the two structures [6], it was difficult to apply the technique to these compounds because the thin-film samples were very small. Therefore, the most useful method to determine their structures was synchrotron radiation (SR)-XRD measurements using the anomalous dispersion effect [8]. At an energy close to the absorption edge, the structure factor changes drastically depending on the energy of the incident X-ray and on the crystal structure. To analyze the crystal structure, we performed SR-XRD measurements while changing the wavelength of the incident X-rays, expecting that the diffraction peak intensities would depend on the crystal structure because of the anomalous dispersion effect.

2. Experimental

CZTS precursors ~1.3 μm thick were deposited by RF magnetron co-sputtering on Mo-coated soda lime glass (SLG) substrates using three targets made of Cu (4N), SnS (4N), and ZnS (4N). The pressure of the Ar sputtering gas was 0.5 Pa. The CZTS films were formed by sulfurizing the CZTS precursors at 580 °C and 540 °C for 3 h. The detailed technique was described in Refs. [9–13]. Three types of CZTS films were investigated, with Cu-rich (C), stoichiometric (S), and Cu-poor (P) compositions. Powder samples were obtained by grinding CZTS flakes, which were scraped off of the CZTS films on the substrates, in an agate mortar. The powders were then placed in a Lindemann capillary with a 0.2 mm inner diameter. Synchrotron X-ray diffraction (XRD) measurements were performed at BL19B2 in SPring-8. The XRD data were recorded on an imaging plate (IP) at ambient temperature. Wavelengths of 0.139–0.150 nm were used to enhance the anomalous dispersion effect close to the Cu K-edge. To prevent the background due to fluorescence X-rays from the samples, an X-ray with a longer wavelength than 0.138 nm, which is the absorption wavelength of the Cu K-edge, was used. It was confirmed that there was no spot pattern in the Debye-ring originating from large grains in the samples. The computer

* Corresponding author. Tel.: +81 561 71 7818; fax: +81 561 63 6448.
E-mail address: h-nozaki@mosk.tytlabs.co.jp (H. Nozaki).

0925-8388/$ – see front matter © 2012 Elsevier B.V. All rights reserved.
doi:10.1016/j.jallcom.2012.01.134

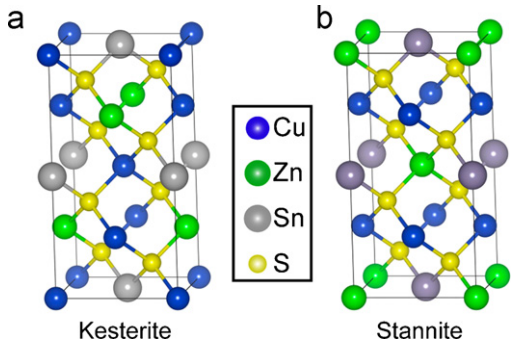

Fig. 1. (a) Kesterite (space group $I\bar{4}$) and (b) stannite (space group $I\bar{4}2m$) crystal structures for CZTS. The crystal structures were drawn by the VESTA computer program [16].

Table 1
The atomic positions in the unit cells of kesterite and stannite structures.

Site	Atomic positions for kesterite	
2*a*	(0, 0, 0)	(1/2, 1/2, 1/2)
2*b*	(0, 0, 1/2)	(1/2, 1/2, 0)
2*c*	(0, 1/2, 1/4)	(1/2, 0, 3/4)
2*d*	(0, 1/2, 3/4)	(1/2, 0, 1/4)
8*g*	(*x*, *y*, *z*)	(*x*+1/2, *y*+1/2, *z*+1/2)
	(*x*, −*y*, *z*)	(*x*+1/2, −*y*+1/2, *z*+1/2)
	(*y*, −*x*, −*z*)	(*y*+1/2, −*x*+1/2, −*z*+1/2)
	(−*y*, *x*, −*z*)	(−*y*+1/2, *x*+1/2, −*z*+1/2)
Site	Atomic positions for stannite	
2*a*	(0, 0, 0)	(1/2, 1/2, 1/2)
2*b*	(0, 0, 1/2)	(1/2, 1/2, 0)
4*d*	(0, 1/2, 1/4)	(1/2, 0, 3/4)
	(0, 1/2, 3/4)	(1/2, 0, 1/4)
8*g*	(*x*, *x*, *z*)	(*x*+1/2, *x*+1/2, *z*+1/2)
	(−*x*, −*x*, *z*)	(−*x*+1/2, −*x*+1/2, *z*+1/2)
	(*x*, −*x*, −*z*)	(*x*+1/2, −*x*+1/2, −*z*+1/2)
	(−*x*, *x*, −*z*)	(−*x*+1/2, *x*+1/2, −*z*+1/2)

program RIETAN-FP [14] was used to simulate XRD patterns of the two structures and to perform the Rietveld analysis [15].

3. Results

3.1. Wavelength dependence of the diffraction intensity

A diffraction peak intensity I is proportional to the square of the structure factor F determined by the crystal structure, and F is described as follows:

$$F(\vec{K}) = \sum_{j=1}^{M} f_j(\vec{K}, \lambda) T_j(\vec{K}) \exp\left(2\pi i \vec{K} \cdot \vec{r}_j\right), \quad (1)$$

where $\vec{K}$, f, M, T, and $\vec{r}$ are the scattering vector, the atomic scattering factor of the jth atom, the number of atoms in the unit cell, the atomic displacement factor, and the atomic position of the jth atom, respectively. In Eq. (1), the atomic scattering factors f are described as an equation $f(\vec{K}, \lambda) = f_0(\vec{K}) + f'(\lambda) + if''(\lambda)$, where f' and f'' are the real and imaginary parts of the atomic scattering factor, respectively. Both f' and f'' are dependent on the incident wavelength λ [8]. On the other hand, the structure factor F is strongly affected by the crystal structure. We calculated the relative intensities of the 0 0 2 and 1 1 0 diffraction peaks for the kesterite and stannite structures using the atomic positions indicated in Table 1. The calculated structure factors are shown in Eqs. (2)–(5).

$$F_{K,002} = 2(f_{2a}T_{2a} + f_{2b}T_{2b} - f_{2c}T_{2c} - f_{2d}T_{2d}) + 8f_{8g}T_{8g}\cos(4\pi z), \quad (2)$$

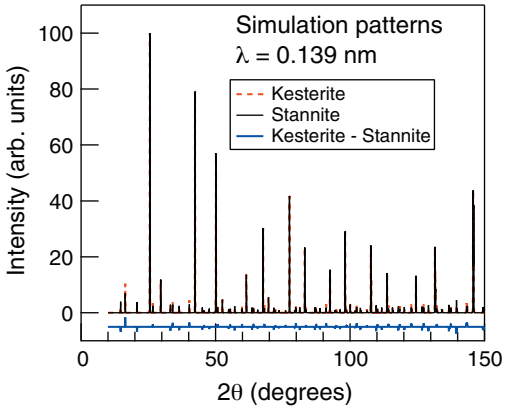

Fig. 2. The XRD simulation patterns of kesterite and stannite structures at a wavelength of 0.139 nm. The intensities were normalized to the maximum peak intensity.

$$F_{S,002} = 2(f_{2a}T_{2a} + f_{2b}T_{2b} - 2f_{4d}T_{4d}) + 8f_{8g}T_{8g}\cos(4\pi z), \quad (3)$$

$$F_{K,101} = 2(f_{2a}T_{2a} - f_{2b}T_{2b} + if_{2c}T_{2c} - if_{2d}T_{2d}) + 2f_{8g}T_{8g}\{\exp[2\pi i(x+z)] + \exp[2\pi i(-x+z)] + \exp[2\pi i(y-z)] + \exp[2\pi i(-y-z)]\}, \quad (4)$$

$$F_{S,101} = 2(f_{2a}T_{2a} - f_{2b}T_{2b}) + 2f_{8g}T_{8g}\left\{\cos[2\pi(x+z)] + \cos[2\pi(-x+z)]\right\}. \quad (5)$$

Here, f_j and T_j denote the atomic scattering factor and atomic displacement factor, respectively. Because the Cu atom occupies the 2*a* and 2*d* sites of the kesterite structure[4], the contribution of Cu atoms to $F_{K,002}$ disappears (see Eq. (2)), while $F_{K,101}$ is affected by the Cu atoms (see Eq. (4)). On the other hand, the Cu atom occupies the 4*d* site of the stannite structure[4], so there is no contribution from Cu atoms to $F_{S,101}$ (see Eq. (5)), while $F_{S,002}$ is affected by the Cu atoms (see Eq. (3)). Therefore, the kesterite and stannite structures can be identified by measuring the wavelength dependences of the 0 0 2 and 1 0 1 peaks around the Cu K-edge, even if the diffraction peak intensity was not measured correctly.

3.2. Simulation of peak intensities

Simulated XRD patterns for the kesterite and stannite structures at wavelength of 0.139 nm are shown in Fig. 2. The subtracted pattern shows that the difference intensity between the kesterite and stannite structures is less than 5%. This indicates that it is difficult to distinguish their crystal structures by Rietveld analysis with the data taken at a single wavelength, because the absolute intensities of the diffraction peaks are easily changed by their orientation or the mixing of large grains. As a result, the diffraction peaks are not sharp enough to allow the precise calculation of the structure factor, due to the small grain size. Therefore, we discriminated the crystal structures using the anomalous dispersion effect.

The wavelength dependencies of the intensity of the 0 0 2 and 1 0 1 diffraction peaks $[I_{002}(\lambda), I_{101}(\lambda)]$ of the kesterite and stannite structures were simulated, as shown in Fig. 3. The peak intensity $I_{002}(\lambda)$ $[I_{101}(\lambda)]$ of the stannite structure decreased by 30% (10%) upon increasing the wavelength from 0.139 nm to 0.150 nm, while the same peaks decreased by 10% (25%) for the kesterite structure. Because of the strong wavelength dependence of $I_{002}(\lambda)$ $[I_{101}(\lambda)]$ for the two types of crystal structure, it is possible to distinguish the structures experimentally, despite contamination by large grains and/or preferred orientation effects.

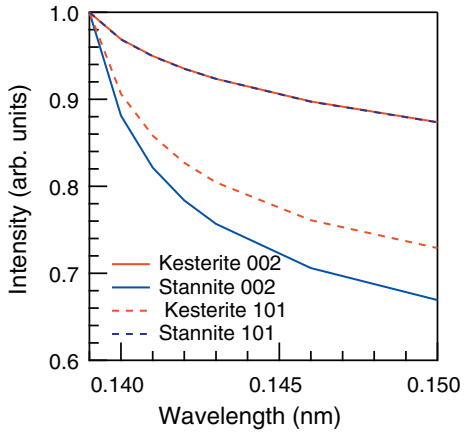

Fig. 3. Simulated wavelength dependencies of the 0 0 2 and 1 0 1 diffraction peak intensities for kesterite and stannite structures. Each peak intensity was normalized to the 1 1 2 main peak intensity. Although the 0 0 2 peak for kesterite and the 1 0 1 peak for stannite seem to have the same behavior, their intensities are slightly different. The real and imaginary components of the anomalous dispersion were reported in Ref. [8].

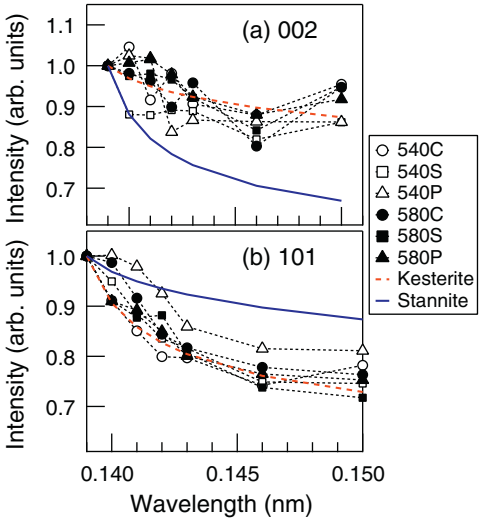

Fig. 4. The wavelength dependence of (a) 0 0 2 and (b) 1 0 1 Bragg peak intensity. The solid lines indicate simulated results. The peak intensities were normalized to that of 0.139 nm.

3.3. XRD data and Rietveld refinement

$I_{002}(\lambda)$ and $I_{101}(\lambda)$ values obtained from the XRD data are shown in Fig. 4. $I_{002}(\lambda)$ and $I_{101}(\lambda)$ decreased monotonically with increasing wavelength along the simulated line for the kesterite structure for all samples. This suggests that the CZTS thin films obtained in this experiment preferred the kesterite structure. Rietveld analysis was performed using the measured data for kesterite. The refined result for a 580S sample is shown in Fig. 5 and Table 2. The difference pattern $I_{obs} - I_{cal}$ had a very small deviation, indicating that the variable parameters were well converged, and the reliability (R) factor was 6.02 %. As shown in Table 2, the occupancies of the 2*a* and 2*b* sites were slightly different from the stoichiometric values of the kesterite structure, while those of the 2*c* and 2*d* sites were almost stoichiometric. The composition ratio was slightly different from the stoichiometric ratio; that is, slightly Cu-poor, Sn-poor, and Zn-rich. The atomic composition ratios were calculated as Cu/(Zn + Sn) = 0.97 and Zn/Sn = 1.42. This result had the same tendency as reported previously on the basis of X-ray fluorescence analysis [9–13]. The bond lengths from the 8*g* site (S) to the 2*a*, 2*b*, 2*c*, and 2*d* sites are indicated in Table 3. The 2*a*–8*g* and 2*d*–8*g* lengths were *ca*. 8% longer than their reported values [18–20]. These longer bond lengths were probably due to disorder of the 2*a* and 2*d* sites, resulting in a large atomic displacement parameter B as shown in Table 2.

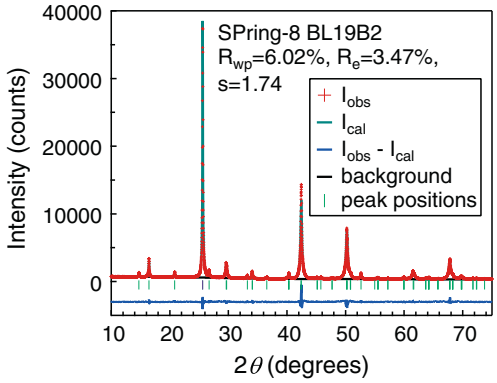

Fig. 5. Rietveld refinement results for a 580S sample. There was a small amount of ZnS phase as an impurity, and the volume fraction was estimated to be ~2%. Therefore it should not have affected the Rietveld refinement.

Table 2
Crystal structure parameters obtained by Rietveld analysis of a 580S sample. Here, *g*, (*x*, *y*, *z*), and *b* indicate the occupancy, the fractional positions, and the atomic displacement parameter, respectively.

Site	Atom	*g*	*x*	*y*	*z*	*B* (nm^2)
2*a*	Cu Zn	0.77(5) 0.23	0	0	0	0.032(2)
2*b*	Sn Cu	0.841(8) 0.159	0	0	1/2	0.0173(3)
2*c*	Cu	1	0	1/2	1/4	0.002
2*d*	Zn Cu	0.96(4) 0.04	0	1/2	3/4	0.06(3)
8*g*	S	1	0.242(2)	0.245(2)	0.1280(4)	0.0258(5)

Space group: $I\bar{4}$, a = 5.4380(1) Å, c = 10.857(3) Å, Rwp = 6.02%, Re = 3.47%, S = 1.74, Cu : Zn : Sn : S = 3.94 : 2.38 : 1.68 : 8.0.

Table 3
The calculated and theoretical bond lengths from the 8*g* (S) site to the 2*a*, 2*b*, 2*c*, and 2*d* sites. The theoretical values were obtained by summing up each atomic radius with a Ref. [17].

	Sites	Bond length (nm)
Present work	2*a* ($Cu_{0.77}Zn_{0.23}$)	0.2337
	2*b* ($Sn_{0.841}Cu_{0.159}$)	0.2403
	2*c* (Cu)	0.2261
	2*d* ($Zn_{0.96}Cu_{0.04}$)	0.2400
Previous reports	Cu–S [18]	0.215
	Zn–S [19]	0.221
	Sn–S [20]	0.243

4. Conclusion

We performed SR-XRD experiments to distinguish the crystal structures of CZTS thin film using the anomalous dispersion effect. The crystal structures were clearly identified as the kesterite structure, although the amount of powder in the sample was very low. Rietveld analysis based on the kesterite structure revealed that the atomic composition ratios were slightly different from the stoichiometric amounts. The detailed crystal structure analysis corresponding to the power conversion efficiency will be published later, with the crystal structure treated as kesterite on the basis of this work. To the author's knowledge, the detailed crystal

structure analysis of CZTS thin films has not been reported elsewhere. Therefore, this result should enable the calculation of the electronic band structure by first-principles calculation, enabling the design of highly efficient solar cell materials.

Acknowledgements

The authors thank Dr. M. Sato and Dr. T. Koganezawa of the Japan Synchrotron Radiation Research Institute (JASRI) for performing XRD measurement. The synchrotron radiation experiment was performed at BL19B2 in the SPring-8 with the approval of JASRI (Proposal No. 2008A1759).

References

[1] H. Katagiri, Thin Solid Films 480–481 (2005) 426.
[2] H. Katagiri, K. Jimbo, S. Yamada, T. Kamimura, W.S. Maw, T. Fukano, T. Ito, T. Motohiro, Appl. Phys. Express 1 (2008) 041201.
[3] K. Ito, T. Nakazawa, Jpn. J. Appl. Phys. 27 (1988) 2094.
[4] S.R. Hall, J.T. Syzmanski, J.M. Stewart, Can. Miner. 16 (1978) 131.
[5] S. Schorr, Thin Solid Films 515 (2007) 5985.
[6] S. Schorr, H.J. Hoebler, M. Tovar, Eur. J. Mineral. 19 (2007) 65.
[7] J. Paier, R. Asahi, A. Nagoya, G. Kresse, Phys. Rev. B 79 (2009) 115126.
[8] L. Kissel, R.H. Pratt, Acta Crystallogr. A 46 (1990) 170.
[9] K. Jimbo, R. Kimura, T. Kamimura, S. Yamada, W.S. Maw, H. Araki, K. Oishi, H. Katagiri, Thin Solid Films 515 (2007) 5997.
[10] K. Oishi, G. Saito, K. Ebina, M. Nagahashi, K. Jimbo, W.S. Maw, H. Katagiri, M. Yamazaki, H. Araki, A. Takeuchi, Thin Solid Films 517 (2008) 1449.
[11] H. Araki, A. Mikaduki, Y. Kubo, T. Sato, K. Jimbo, W.S. Maw, H. Katagiri, M. Yamazaki, K. Oishi, A. Takeuchi, Thin Solid Films 517 (2008) 1457.
[12] H. Araki, Y. Kubo, A. Mikaduki, K. Jimbo, W.S. Maw, H. Katagiri, M. Yamazaki, K. Oishi, A. Takeuchi, Sol. Energy Mater. Sol. Cells 93 (2009) 996.
[13] H. Katagiri, K. Jimbo, W.S. Maw, K. Oishi, M. Yamazaki, H. Araki, A. Takeuchi, Thin Solid Films 517 (2009) 2455.
[14] F. Izumi, K. Momma, Solid State Phenom. 130 (2007) 15.
[15] H.M. Rietveld, J. Appl. Cryst. 2 (1969) 65.
[16] K. Momma, F. Izumi, J. Appl. Cryst. 41 (2008) 653.
[17] P. Pyykko, M. Atsumi, Chem. Eur. J. 15 (2009) 186.
[18] H. Fjellvåg, F. Grønvold, S. Stølen, A.F. Andresen, R. Müller-Käfer, A. Simon, Z. Kristallogr. 184 (1988) 111.
[19] Chin-Yu Yeh, Z.W. Lu, S. Froyen, A. Zunger, Phys. Rev. B 46 (1992) 10086.
[20] R.W.G. Wyckoff, Crystal Structures, vol. 85, second edition, Interscience Publishers, New York, NY, 1963.